Reconstructing Sparticle Mass Spectra using Hadronic Decays

J. M. Butterworth[1], John Ellis[2] and A. R. Raklev[2,3]

[1] Department of Physics & Astronomy, University College London
[2] Theory Division, Physics department, CERN
[3] Department of Physics & Technology, University of Bergen

Abstract

Most sparticle decay cascades envisaged at the Large Hadron Collider (LHC) involve hadronic decays of intermediate particles. We use state-of-the art techniques based on the $K_\perp$ jet algorithm to reconstruct the resulting hadronic final states for simulated LHC events in a number of benchmark supersymmetric scenarios. In particular, we show that a general method of selecting preferentially boosted massive particles such as $W^\pm, Z^0$ or Higgs bosons decaying to jets, using sub-jets found by the $K_\perp$ algorithm, suppresses QCD backgrounds and thereby enhances the observability of signals that would otherwise be indistinct. Consequently, measurements of the supersymmetric mass spectrum at the per-cent level can be obtained from cascades including the hadronic decays of such massive intermediate bosons.

1 Introduction

In a number of commonly considered supersymmetric (SUSY) models, strongly-interacting sparticles will be abundantly pair-produced at the Large Hadron Collider (LHC), and the resulting events containing jets and missing energy will stand out above the Standard Model background. The next challenge will be to make sense of the events, which will typically involve cascade decays through several intermediate sparticles. It will be particularly desirable to obtain information on the SUSY masses and branching ratios. It has been demonstrated that cascades involving lepton emission often provide relatively clean signals, which can be used to reconstruct several sparticle masses in some favourable benchmark scenarios, see e.g. [1, 2]. However, these decay channels often suffer from branching ratios that are low compared to hadronic decay modes, reducing the available sample size and therefore restricting access to high-mass sparticles. Moreover, the charged leptons are often associated with neutrinos, for example in chargino ($\chi^{\pm}$) decays. The presence of the neutrinos would confuse the interpretation of the missing-energy signal provided by escaping neutralinos in scenarios with R-parity conservation, as we assume here, and make the reconstruction of chargino masses difficult. Some progress on techniques for measuring chargino masses has been reported for scenarios with one leptonic and one hadronic decay chain [3], but these require models with a favourable combination of the corresponding branching ratios. The ability to reconstruct purely hadronic cascade decays would facilitate the discovery and measurement of charginos in more general cases, as well as enable heavier sparticle masses to be reconstructed.

In this paper, we take a new approach to the reconstruction of fully-hadronic sparticle events, starting from the missing-energy signal provided by the neutralino in R-conserving models, which suppresses Standard Model (SM) backgrounds. We use jet analysis techniques based on the $K_{\perp}$ algorithm to identify the hadronic decays of massive bosons such as the $W^{\pm}$, Z^0 or Higgs boson (h). In general, the majority of sparticle cascade decays yield fully-hadronic final states containing such massive SM particles decaying to $q - \bar{q}$ jet pairs [4]. A certain fraction of these bosons, dependent on the sparticle masses in the scenario considered, are highly boosted and the jets from the decays are closely aligned, indeed overlapping, in pseudo-rapidity (η) - azimuthal angle (ϕ) space. Such a situation presents both a challenge and an opportunity. The challenge is that the choice of jet finder becomes crucial: the treatment of jet overlaps can be sensitive to rather soft and subtle QCD effects, and yet somehow one needs to retain the information that the jet arises from the two-body decay of a massive particle. The opportunity is that, since the jets are close together, there is no combinatorial background; no need, for example, to combine all pairs of jets to see if they reconstruct to the W mass.

We address the reconstruction issue using the sub-jet technique that was proposed

previously as a way to identify high-energy WW events [5]. This technique and its extension to hadronic sparticle decays are described in Section 2. Then, in Section 3 some specific benchmark SUSY scenarios and the specific decay chains of interest are described: these involve typical decays of intermediate heavy charginos or neutralinos such as $\tilde{\chi}_1^\pm \to W^\pm \tilde{\chi}_1^0$ and $\tilde{\chi}_2^0 \to Z^0, h\tilde{\chi}_1^0$. The simulations and analysis method are described in Section 4, and the subsequent Section contains the results and conclusions.

2   Jet Finding and Sub-jets

The identification of jets which originate from a decaying massive particle begins by using a jet algorithm to define the jet. In this analysis the $K_\perp$ algorithm [6] is used, in the inclusive mode with the E reconstruction scheme. For each particle k and pair of particles (k, l), the algorithm calculates the quantities

$$
\begin{aligned}
d_{kB} &= p_{Tk}^2, \\
d_{lB} &= p_{Tl}^2, \\
d_{kl} &= \min(p_{Tk}^2, p_{Tl}^2) R_{kl}^2 / R^2,
\end{aligned}
\tag{1}
$$

where p_{Tk} is the transverse momentum of particle k with respect to the beam axis and

$$
R_{kl}^2 = (\eta_k - \eta_l)^2 + (\phi_k - \phi_l)^2.
\tag{2}
$$

The parameter R is a number of order one. If it is set below unity, it is less likely that a given particle will be merged with a jet, which in turn leads to narrower jets. Thus R plays a somewhat similar role to the adjustable cone radius in cone algorithms. In this analysis, initial studies indicated that $R = 0.7$ provided a good compromise between efficiency and the mass resolution, and this value is used throughout. Returning to the algorithm: all the d values are then ordered. If d_{kB} or d_{lB} is the smallest, then particle k or l is labelled a jet and removed from the list. If d_{kl} is the smallest, particles k and l are merged by adding their four-momenta. The list is recalculated and the process is repeated until the list is empty. Thus the algorithm clusters all particles into jets, and a cut on transverse momentum can then be used to select the hardest jets in the event. The algorithm is infrared safe, and has the additional benefit that each particle is uniquely assigned to a single jet. Recently a fast implementation of the algorithm has been developed [7] which makes it practical for use even in the very high multiplicity events expected at the LHC.

In selecting a candidate for a hadronic decay of the $W^\pm$, Z^0 or h, first cuts on the p_T and the pseudo-rapidity (η) of the jet are applied so as to ensure that they are energetic enough to contain a boosted heavy-particle decay and are in a region of

good detector acceptance. A cut is then applied on the mass of the jet (calculated from the four-vectors of the constituents) to ensure that it is in a window around the nominal mass of the desired particle.

The next step is to force the jet to decompose into two sub-jets. The main extra piece of information gained from the sub-jet decomposition is the y cut at which the sub-jets are defined: $y \equiv d_{kl}/(p_T^{\text{jet}})^2$, where p_T^{jet} is the transverse momentum of the candidate jet containing the sub-jets k and l. In the case of a genuine $W^\pm, Z^0$ or h decay, the expectation is that the scale at which the jet is resolved into sub-jets (i.e., yp_T^2) will be $\mathcal{O}(M^2)$, where M is the $W^\pm, Z^0$ or h mass. For QCD jets initiated by a single quark or gluon, the scale of the splitting is expected to be substantially below p_T^2, i.e., $y \ll 1$, since in the region around the jet strongly-ordered DGLAP-like [8] QCD evolution dominates.

This distinction provides new information in addition to the jet mass itself, as is illustrated in Figures 1a and 1b, where the correlation between the jet mass and the splitting scale is shown for $W^\pm$ jets and QCD jets respectively. The events shown are $W^\pm$+jet events and SUSY events generated using PYTHIA 6.408 [9], and $W^\pm$+3jet events generated using ALPGEN [10] for the matrix element, HER-WIG 6.510 [11] for parton showering and JIMMY [12] for the underlying event. The parameters for the underlying event and the parton showers were those of the ATLAS tune of PYTHIA and the CDF tune A of HERWIG and JIMMY, taken from [13] [1]. These models have been shown to give a good description of a wide variety of data. In particular, the modelling of the internal jet structure by leading-logarithmic parton showers is known to be good for jets produced in $p\bar{p}$ collisions [14], ep collisions and photo-production [15], and in e^+e^- annihilation events and $\gamma\gamma$ collisions [16].

Although there are some differences between the results of the PYTHIA and HER-WIG/ALPGEN simulations, the conclusions are similar. Fig. 1a confirms that the splitting scale in $W^\pm$ decays is relatively large, typically ≥ 20 GeV, whereas Fig. 1b shows that the splitting scale for QCD jets with masses ~ 80 GeV is typically ≤ 20 GeV. The distributions of of $p_T\sqrt{y}$ and of y are shown in Figures 1c and 1d for $W^\pm$ jets and QCD jets. The distributions are qualitatively similar, whether they are generated in SUSY events or in conventional $W^\pm$+jets events, and whether (in the latter case) they are generated using PYTHIA or HERWIG. The scale of the splitting is seen to be peaked close to the $W^\pm$ mass for genuine $W^\pm$ decays, whichever the environment in which they are produced, and to be softer for QCD jets which just happen to reconstruct to the $W^\pm$ mass, again in both environments.

This distinction was noted and successfully used to identify $W^\pm$ decays in simulations of W^+W^- scattering at LHC energies in [5]. Here, this information is used in

---

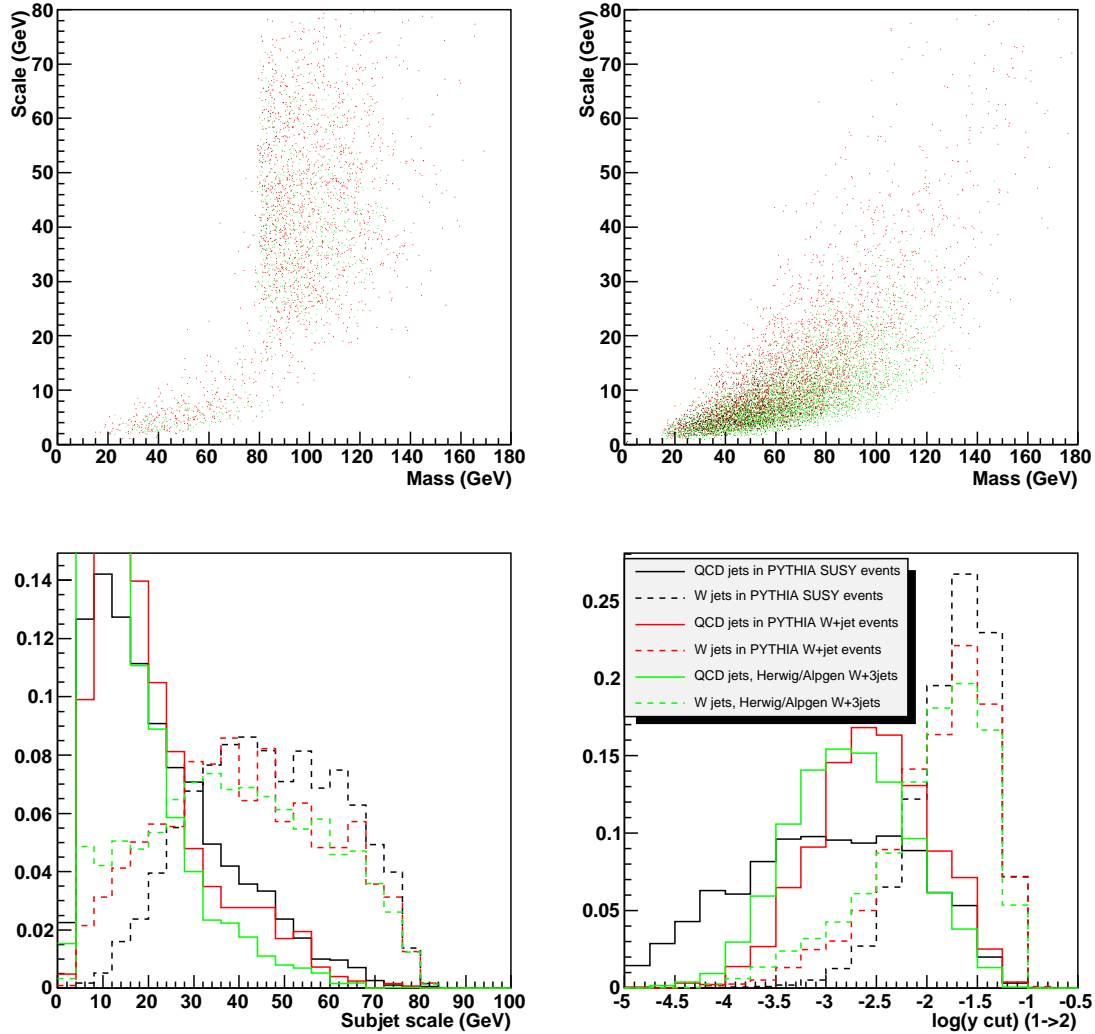[1]More details on the SUSY event generation are given in Section 4.

3

Figure 1: Scatter plot of the jet mass against the jet splitting scale yp_T^2 for (a) jets from $W^\pm$ decays (determined by a match better than 0.1 units in $\eta - \phi$) and (b) QCD jets in $W^\pm$+jet and SUSY events. The distributions of the splitting scale are shown in (c) and the y distributions in (d), for the same types of jets, after a cut on the jet mass at $75 < M < 90$ GeV. In all these plots, the requirement $p_T > 250$ GeV is applied to all jets. The histograms in the lower two plots are normalised to unity.

4

the analysis described in Section 4 to refine the selection of $W^\pm$, Z^0 and h candidates in sparticle decay cascades. Although no detector simulation is employed in this analysis, the cut on the scale has been shown previously to be robust against the effects of the underlying events [5], as well as effects due to the calorimeter granularity and resolution [17].

3 SUSY Decay Chains and Benchmark Scenarios

The pair-production of heavy sparticles in generic SUSY models yields on-shell electroweak gauge bosons or Higgs bosons via the decays of heavy gauginos that appear as intermediate steps in cascades, e.g., $\tilde{q}_L \to \tilde{\chi}_2^0 q$ or $\tilde{q}_L \to \tilde{\chi}_1^\pm q'$, followed by $\tilde{\chi}_2^0 \to Z^0, h + \tilde{\chi}_1^0$ or $\tilde{\chi}^\pm \to W^\pm + \tilde{\chi}_1^0$ decays. Exceptions are cases with gaugino masses that are nearly degenerate, in which there may be large branching ratios for decays via off-shell heavy bosons. Since the largest branching ratios for $W^\pm$, Z^0 and h decays are those into hadronic $\bar{q}q$ final states, purely hadronic final states dominate in cascade decays via on-shell bosons, and these are also potentially important in off-shell decays.

For the decay chain

$$\tilde{q}_L \to \tilde{\chi}_1^\pm q' \to \tilde{\chi}_1^0 W^\pm q' \tag{3}$$

shown in Fig. 2, one can demonstrate that the invariant mass distribution of the quark-W system has a minimum and maximum given by

$$(m_{qW}^{\mathrm{max/min}})^2 = m_W^2 + \frac{(m_{\tilde{q}_L}^2 - m_{\tilde{\chi}_1^\pm}^2)}{m_{\tilde{\chi}_1^\pm}}(E_W \pm |\vec{p}_W|), \tag{4}$$

where

$$|\vec{p}_W|^2 = \frac{(m_{\tilde{\chi}_1^\pm}^2 - m_{\tilde{\chi}_1^0}^2 - m_W^2)^2 - 4m_{\tilde{\chi}_1^0}^2 m_W^2}{4m_{\tilde{\chi}_1^\pm}^2} \tag{5}$$

is the W momentum in the chargino rest frame. If measurable, these endpoints give a model-independent relationship between the three SUSY masses, modulo the existence of the decay chain. If both endpoints can be determined experimentally, the squark mass can be eliminated, giving the chargino mass in terms of the lightest neutralino. Supplementary model-dependent assumptions, such as the relationship $m_{\tilde{\chi}_1^\pm} \approx 2m_{\tilde{\chi}_1^0}$ that holds approximately in the constrained MSSM (CMSSM), can then be used to determine individual masses of all three sparticles in specific theoretical frameworks.

The decay chains

$$\tilde{q}_L \to \tilde{\chi}_2^0 q \to \tilde{\chi}_1^0 h q \tag{6}$$
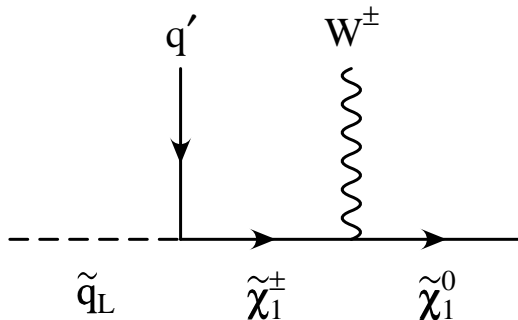
Figure 2: The SUSY decay chain of Eq. (3).

and

$$\tilde{q}_L \rightarrow \tilde{\chi}_2^0 q \rightarrow \tilde{\chi}_1^0 Z^0 q, \tag{7}$$

involving the second lightest neutralino, have endpoint formulae with the same structure, given by the substitutions

$$W \rightarrow h, \quad \tilde{\chi}_1^\pm \rightarrow \tilde{\chi}_2^0 \tag{8}$$

and

$$W \rightarrow Z, \quad \tilde{\chi}_1^\pm \rightarrow \tilde{\chi}_2^0, \tag{9}$$

respectively, in Eqs. (4) and (5).

In [4] benchmark models with such cascade decays were explored in a more generic setting than that allowed in the CMSSM. Relaxing the GUT-scale universality of the Higgs scalar masses or introducing a gravitino dark matter candidate admits values of the (supposedly universal) scalar squark and slepton mass m_0 outside the narrow range allowed by the cold dark matter density [18, 19] within the restrictive CMSSM framework. This, in turn, allows for a wide range of values for the branching ratios of the lightest chargino and the next-to-lightest neutralino into $W^\pm, Z^0$ and h. In our study, we use the benchmark points α, β, γ and δ from [4] to illustrate these possibilities. The points α, β, γ are scenarios with relatively light SUSY masses, that should be easy to probe at the LHC, while δ represents a more challenging scenario with lower cross sections. Common to all four points is the large branching ratio for squark to chargino/neutralino decays, $\text{BR}(\tilde{q}_L \rightarrow \tilde{\chi}_1^\pm q) \approx 60\%$ and $\text{BR}(\tilde{q}_L \rightarrow \tilde{\chi}_2^0 q) \approx 30\%$. The corresponding chargino and neutralino bosonic branching ratios are shown in Table 1.

We show the predicted shape of the invariant mass distributions for the kinematically-allowed quark-boson combinations in the decay chains (3), (6) and (7), for all the considered benchmark points, in Fig. 3. These distributions consider only the kinematics of the decay chain and assume zero width for all particles. The

6

Point/BR	$\tilde{\chi}_2^0 \to \tilde{\chi}_1^0 Z$	$\tilde{\chi}_2^0 \to \tilde{\chi}_1^0 h$	$\tilde{\chi}_1^\pm \to \tilde{\chi}_1^0 W^\pm$
α	98.6	0.0	99.6
β	7.5	64.5	79.0
γ	0.0	0.0	99.9
δ	5.4	92.0	97.5

Table 1: Branching ratios for $\tilde{\chi}_2^0$ and $\tilde{\chi}_1^\pm$ in the selected SUSY benchmark models. The decays are calculated using SDECAY 1.1A [20].

distributions have a characteristic trapezoidal shape with only small variations in the location of the upper edge with the changing boson mass. This similarity is due to the neutralino/chargino mass degeneracy typical in CMSSM models, and demonstrates that the upper endpoint given by Eq. (4) is to a large extent insensitive to the boson mass. Locating the upper endpoints for two different decay chains involving the chargino and neutralino, respectively, would be an excellent test of this mass degeneracy. If they are similar, this would point towards SUSY scenarios where both the second-lightest neutralino and the lightest chargino are 'wino-like'.

4   Simulation and Analysis

4.1   Simulation

In order to simulate sparticle pair-production events at the LHC, we use PYTHIA 6.408 [9] with CTEQ 5L PDFs [21] interfaced to HZTOOL [22], with some minor changes to allow for simulations of SUSY scenarios. Decay widths and branching ratios for the SUSY particles are calculated with SDECAY 1.1A [20]. For the α, β and γ benchmark points we simulate a number of SUSY events equivalent to 30 fb^{-1}, giving results that should be representative of the early reach of the LHC experiments at low luminosity. For the δ benchmark point, with its considerably higher masses and lower cross sections, we simulate a number of events equivalent to 300 fb^{-1}, yielding results that should indicate the ultimate reach of the LHC experiments with their design luminosity.

We have also generated SM backgrounds with PYTHIA in five p_T bins from $p_T = 50$ GeV to 7 TeV. These samples rely on the parton shower to simulate extra jets. This should be a reasonable approximation in the important kinematic regions for some processes, such as $t\bar{t}$, where the scale of the hard interaction is > 350 GeV and we rely on parton showers to simulate jets at around 150-200 GeV. However, this is not adequate in all cases, and so in addition we have investigated other possibly
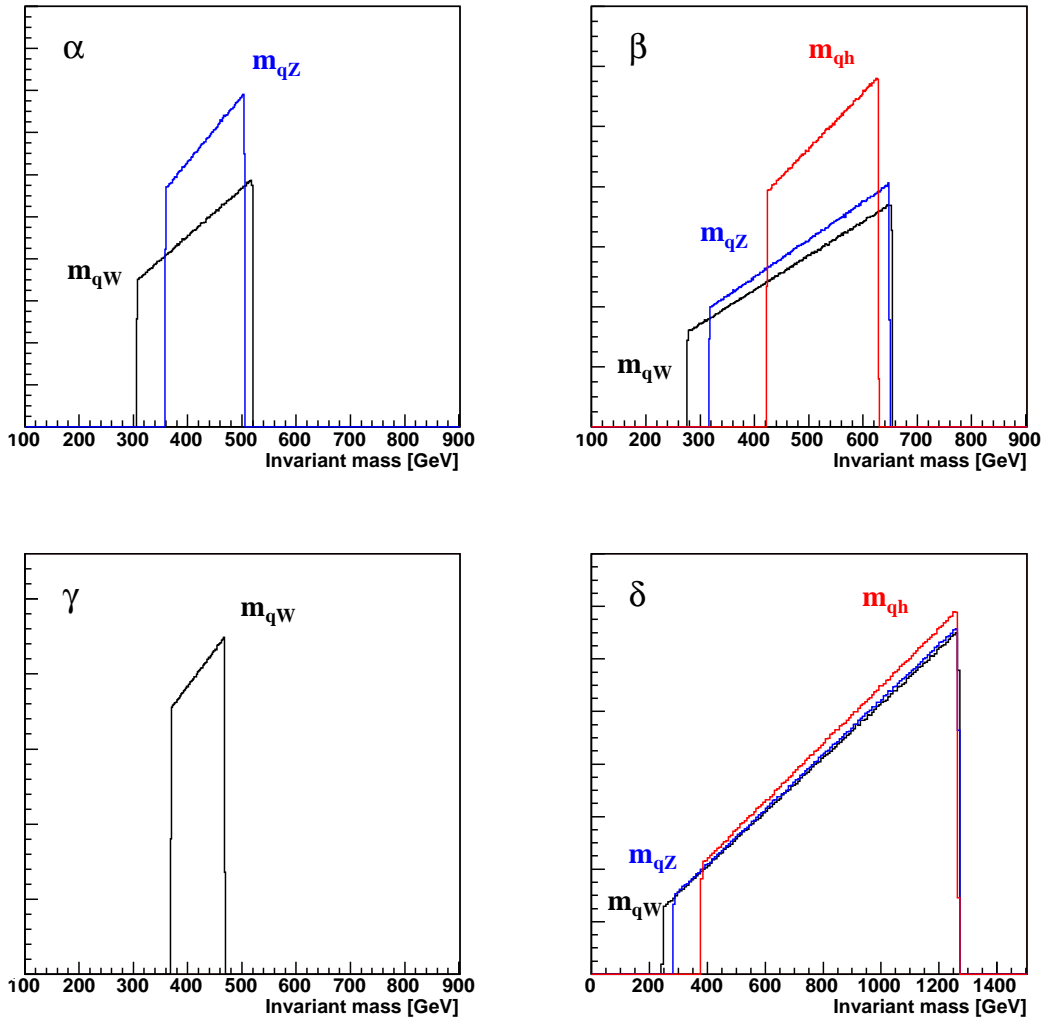
Figure 3: The invariant mass distributions of $qW^{\pm}$, qZ and qh combinations for the chosen SUSY benchmark points.

important sources of background, by using ALPGEN/HERWIG to generate final states containing dibosons plus one or two jets, or a single boson plus two or three jets [2]. In these cases the jet multiplicities are not well modelled by parton showers, but the internal jet structure should still be well described. These backgrounds turn out not to be very important for the α, β and γ scenarios, but are found to be significant in the δ scenario due to the small SUSY production cross section. For the multiple jet processes there is a small amount of double counting with the PYTHIA samples, which we neglect here, giving a conservative estimate of the backgrounds in this sense. The generated numbers of events for the various processes, per p_T bin where used, are shown in Table 2 along with the corresponding integrated luminosities.

No attempt to simulate detector effects has been made, but we have included semi-realistic geometrical requirements for jets and leptons, restricting ourselves to leptons with $|\eta| < 2.5$ and jets with $|\eta| < 4.0$ [3]. We calculate the missing transverse energy from the vector sum of the momenta of all the visible particles within $|\eta| < 5.0$, excluding neutrinos and neutralinos. For our investigation of Higgs decays into $b\bar{b}$ pairs we use a simple statistical model for identifying two collimated b-jets, by tagging any jet matched to the direction of two b quarks with $p_T > 15$ GeV at the parton level [4] as resulting from two collimated b-jets with an efficiency of 40%, and using a mis-tagging rate of 1% for all other jets. The numbers used are a naive estimate from single b-jet tagging at the LHC. More exact predictions for the performance of the LHC detectors on such jets will require the full simulation of a detector, which is beyond the scope of this study.

4.2   Signal Isolation

In order to isolate events with the decay chain (3), we use the following cuts:

- Require missing energy $\not{E}_T > 300$ GeV;

- Require at least one $W^{\pm}$ candidate jet with

    - transverse momentum $p_T > 200$ GeV,
    - jet mass around the W mass: $75 < m_W < 105$ GeV,
    - separation scale $1.5 < \log{(p_T\sqrt{y})} < 1.9$;

---

[2]Appropriate cuts, considering the final-state selections to be used in Section 4.2, have been applied to the partons to reduce the amount of event generation required, and the ALPGEN parton-shower matching scheme was used where appropriate.

[3]Details of the jet reconstruction were given in Section 2.

[4]For a match we require a distance to the jet of less than 0.4 units in the (η, ϕ) plane for each b quark.

Sample	$N_{\text{generated}}$	$\mathcal{L}$ [fb^{-1}]	$N_{\text{pass}}(\alpha - \gamma)$	$N_{\text{pass}}(\delta)$
$t\bar{t}$			256.7	1287.0
50-150	26,500,000	93.0		
150-250	10,000,000	95.6		
250-400	3,500,000	120.0		
400-600	500,000	129.6		
600-	500,000	902.4		
Wj			5.2	34.5
50-150	1,100,000	0.1		
150-250	1,100,000	2.9		
250-400	1,100,000	20.2		
400-600	1,100,000	154.3		
600-	600,000	507.2		
Zj			3.2	3.0
50-150	100,000	0.0		
150-250	100,000	0.6		
250-400	100,000	4.3		
400-600	100,000	32.7		
600-	100,000	199.7		
Wjj	157,800	114.5	49.2	450.5
Zjj	112,000	99.9	43.9	417.7
$Wjjj$	50,300	227.9	127.8	1109.4
$Zjjj$	27,300	156.6	194.4	1782.9
$WW/WZ/ZZ$			9.6	95.3
50-150	100,000	1.8		
150-250	100,000	29.2		
250-400	100,000	158.2		
400-600	100,000	945.2		
600-	10,000	437.0		
WWj	201,200	100.7	9.8	98.3
WZj	162,400	90.2	0.0	0.0
ZZj	69,500	426.5	2.3	17.6
$WWjj$	107,300	98.7	23.4	215.8
$WZjj$	179,000	248.4	55.2	455.5
$ZZjj$	18,900	167.0	5.9	59.3

Table 2: The numbers of generated events, separated by p_T bin where used, the corresponding integrated luminosities and the numbers of events passing the cuts for the qW distribution, as described in Section 4.2. Not shown are $2 \to 2$ QCD events, which are found not to contribute.

10

- Veto events with a top candidate, i.e. a jet-W combination with invariant mass in the range $150 - 220$ GeV.

- Require two additional jets with $p_T > 200, 150$ GeV;

- Veto events containing leptons (e or μ) with $p_T > 10$ GeV.

The asymmetric cut on jet mass is due to the tendency of the jet algorithm to overestimate the jet mass and energy by including contributions from the underlying event and parton shower. Jets which pass the jet mass cut for W candidates are re-calibrated to the known W mass by rescaling the four-vector. To find the invariant $qW^{\pm}$ mass in events that pass all the cuts we combine the $W^{\pm}$ candidate with any jet that passes the $p_T > 200$ GeV requirement. This creates some combinatorial background from signal events where we have picked the wrong jet.

The remaining non-SUSY background is mainly a mix between $t\bar{t}$ events and vector boson (single and pair) production in association with multiple jets. We show the surviving number of events for the given cuts and integrated luminosities in Table 2. While this background is relatively unimportant for the benchmarks with larger cross sections, it is highly significant for the δ benchmark. Thus we have imposed one further cut for this benchmark:

- Require that the angle in the transverse plane between the missing momentum and the W candidate is larger than $\pi/8$.

The reason for this cut is that a significant fraction of the surviving $t\bar{t}$ events feature the $W \to \tau\nu_\tau$ decay of a highly boosted W, where the τ subsequently decays hadronically. This gives large amounts of missing energy from neutrinos, and the possibility of misidentifying the τ jet, or a collimation of the τ jet and the b jet from the same top as the W candidate. The result is a strong correlation between the missing momentum and the direction of the W candidate for the $t\bar{t}$ background.

For the other two decay chains, (6) and (7), we use the same signal extraction procedure, replacing the cut values for the jet mass cut and the separation scale cut with appropriate values. For Z candidates we require $90 < m_Z < 115$ GeV and $1.6 < \log\left(p_T\sqrt{y}\right) < 2.0$, while for the Higgs boson we require $110 < m_h < 140$ GeV and $1.8 < \log\left(p_T\sqrt{y}\right) < 2.1$. In the Higgs case, we further require b-tagging as described in the previous Section, while we do not implement the lepton veto. For our mass reconstruction in Section 4.5 we also look at the relatively clean signal of leptonic Z decays. We keep the cuts on missing energy and additional jets and require two opposite-sign, same-flavour leptons with $p_T > 10$ GeV and an invariant mass in the range $85 - 95$ GeV.

4.3 Invariant Mass Distributions

The resulting invariant $qW^{\pm}$ mass distribution for the α benchmark point is shown in Fig. 4a, for our simulation of 30 fb^{-1}. There is a clear signal peak from events that contain the decay chain (3), above a fairly smooth SUSY background and a small SM background. Their sum yields the black points, with the statistical errors also shown. The SUSY background has a small peak under the signal peak. This is due to a large number of events with misidentification of Zs from neutralino decays as Ws, which can be understood from the neutralino branching ratio in Table 1. We see immediately the remnant of an edge effect at $m_{qW} \sim 500$ GeV, as expected from the true invariant mass distribution shown in Fig. 3. However, the lower edge of the trapezoidal distribution in Fig. 3 at $m_{qW} \sim 300$ GeV is not visible, largely as a result of the hard cuts used on jet momenta. For comparison, we also show in Fig. 4b the corresponding distribution for the $qW^{\pm}$ mass distribution if the cut on the separation scale is *not* imposed: the edge structure is less significant, though still clearly present, with the SUSY background being larger relative to the signal.

The ℓq invariant mass distribution resulting from $W^{\pm} \to \ell^{\pm}\nu$ decays is shown in Fig. 4c: here we have required a lepton (e or μ) with $p_T > 40$ GeV instead of the W-jet cuts. Due to the smearing from the escaping neutrino, there is no interesting edge structure in the signal, and the lack of any efficient cuts other than the p_T of the lepton means that the background dominates. While there may be some information to be gained from the peak positions of the distribution, the leptonic decay is clearly more difficult to use than the hadronic decay utilising the $K_{\perp}$ jet algorithm.

We also show the corresponding invariant mass distribution for qZ^0 combinations followed by Z^0 decays into hadrons in Fig. 4d, and for leptonic Z^0 decays in Fig. 4e. For the hadronic decay the small mass difference between the W and Z means that the signal events (blue) containing the decay chain (7) are swamped by a large SUSY background consisting of events with a misidentified W, despite the higher cut values for jet mass and separation scale.

In the case of leptonic Z decays the background can be reduced much more effectively, by selecting same-flavour, opposite-sign lepton pairs. As with the jets, this pair is rescaled to the known Z mass. The resulting distribution exhibits the expected signal peak for qZ combinations (blue), smeared by combinatorial effects from picking the incorrect jet, over a smaller SUSY background.

Finally, in Fig. 4f we show the invariant qh mass distribution, where there is, as expected, no signal because of the zero branching ratio of the α benchmark.

The corresponding distributions for benchmark β are shown in Fig. 5, again for a simulation of 30 fb^{-1}. We see in panel (a) the expected distinctive edge structure (blue, solid) rising above the SUSY background: the SM background is again small.
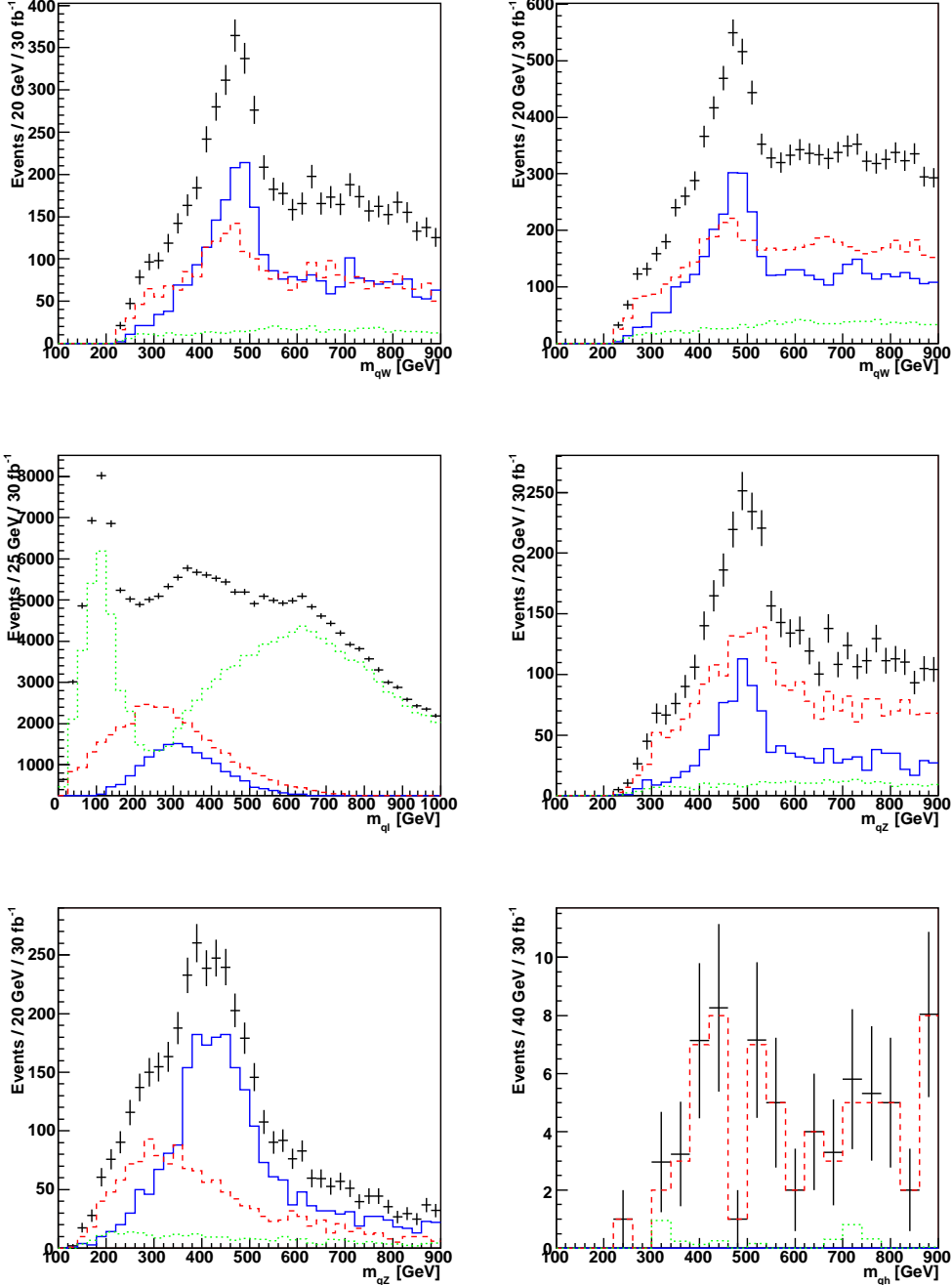
Figure 4: Invariant mass distributions for SUSY benchmark scenario α: combinations of jets and $W^{\pm}$ candidates (a) with and (b) without the cut on the separation scale, (c) the ℓq invariant mass distribution resulting from $W^{\pm} \rightarrow \ell^{\pm}\nu$ decays, combinations of jets and Z^0 bosons decaying (d) hadronically and (e) leptonically, and (f) combinations of jets and h bosons. Signal - blue, solid lines; SUSY background - red, dashed lines; SM background - green, dotted lines.

13

As in the case of benchmark α, we see in panel (b) that the signal-to-background ratio is worse if the cut on the separation scale is *not* imposed. We also observe that the SUSY background has *no* visible peak in the signal peak region, due to the small branching ratio of the neutralino to Z for the β benchmark. Panel (c) of Fig. 5 shows that, as in the case of benchmark α, it would be very difficult to extract information from a leptonic W-decay signal. Nor, according to panels (d) and (e), does it seem possible in the case of benchmark β to extract a Z-decay signal, at least at the considered integrated luminosity. This might have been anticipated because of the much smaller $\tilde{\chi}_2^0 \rightarrow \tilde{\chi}_1^0 Z$ branching ratio in this case compared to the α benchmark.

For the qh distribution in panel (f) the situation is far better. We see a clear edge in the distribution in the expected region of $m_{qh} \sim 650$ GeV. The statistics are low, and are naturally dependent on the b-tagging efficiency. In addition, the observation of the edge relies on the use of the sub-jet separation scale cut. Given the good signal-to-background ratio apparent after this cut, we expect that a lower b-tagging efficiency could be compensated by higher statistics.

In the case of benchmark γ, shown in Fig. 6, also for a simulation of 30 fb^{-1}, we expect only one observable distribution. We see again the familiar features of a strong hadronic W-decay signal with the cut on the separation scale in panel (a) and a weaker signal-to-background ratio without this cut in panel (b). Again there is a peak in the SUSY background under the signal peak. For γ the on-shell decay $\tilde{\chi}_2^0 \rightarrow \tilde{\chi}_1^0 Z$ is not allowed kinematically, but proceeds off-shell and the decay products are again misidentified as Ws. As expected, there are no detectable signals in leptonic W decay, in hadronic or leptonic Z decay, or in hadronic h decay.

We turn finally to the case of benchmark δ, shown in Fig. 7. We recall that in this case the simulation corresponds to an integrated luminosity of 300 fb^{-1}, in view of the higher masses of the sparticles and hence the lower cross sections. We see in panel (a) that the hadronic W-decay signal is less clear in this case, and that for the first time the SM background dominates over that due to SUSY. There are virtually no signal events in panels (c, d) and (e), corresponding to leptonic W decays, hadronic and leptonic Z decays, respectively. However, there is a possible h signal in panel (f). The limited amount of generated events for the SM backgrounds results in relatively large weights for the background at this integrated luminosity, obfuscating the edge structure. We again emphasise the necessity of the sub-jet scale cut and the dependence on the b-tagging efficiency assumed.

4.4   Sideband Subtraction

In order to be able to measure the positions of the expected edges of the invariant mass distributions for signal events, and hence constrain the sparticle masses, we
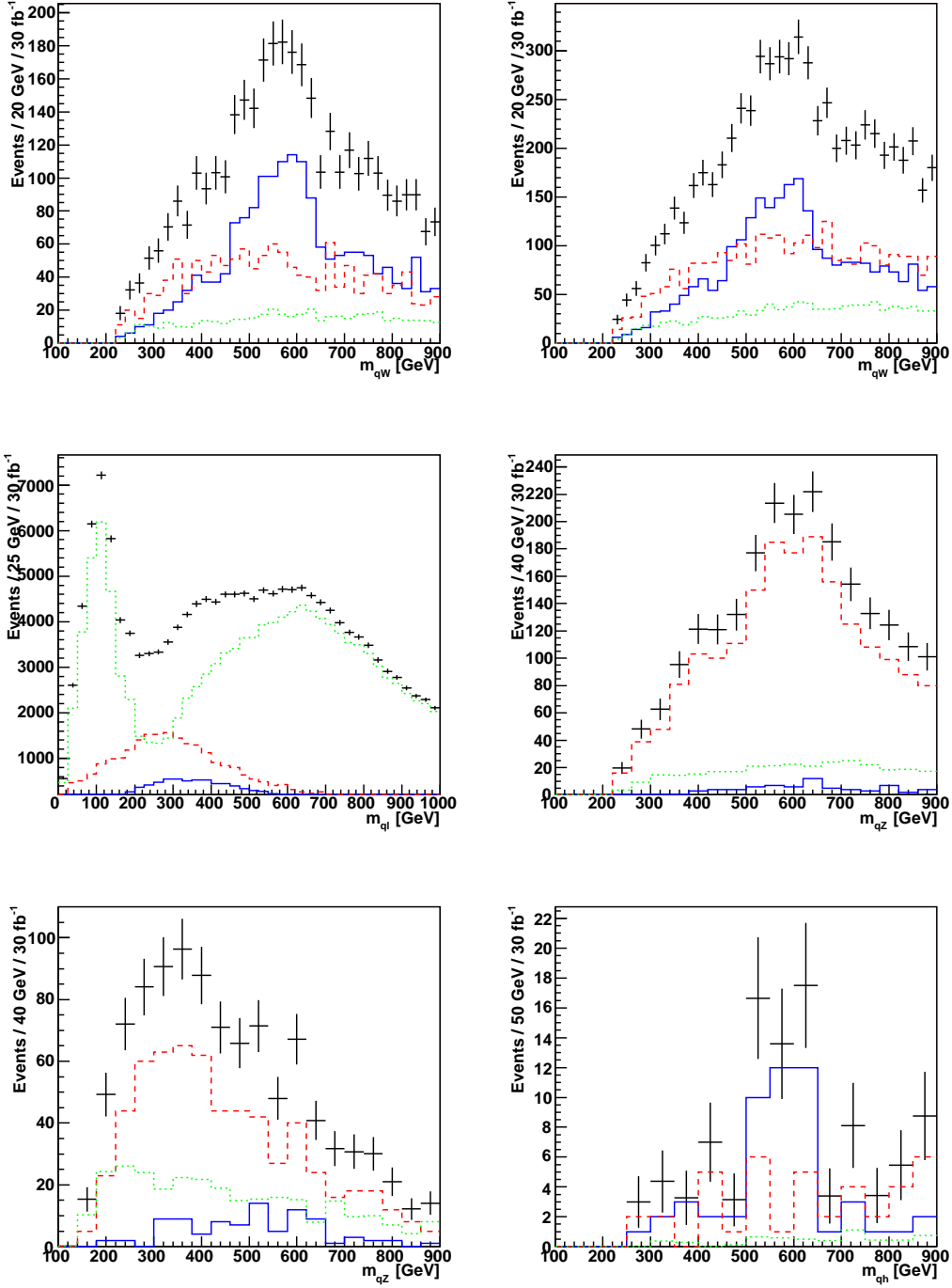
Figure 5: Various invariant mass distributions obtained in a simulation of events for SUSY benchmark scenario β. See Fig. 4 and text for details.
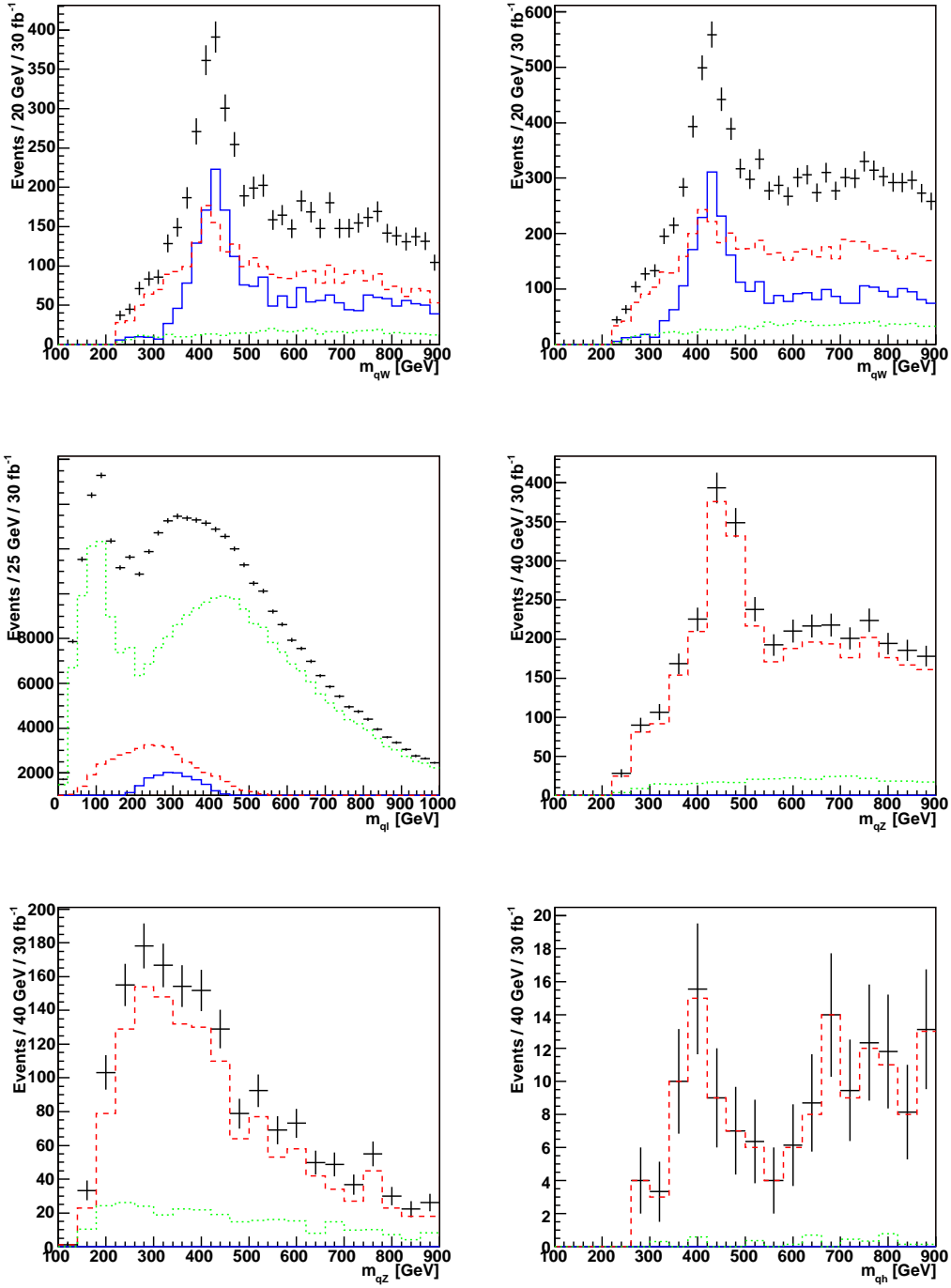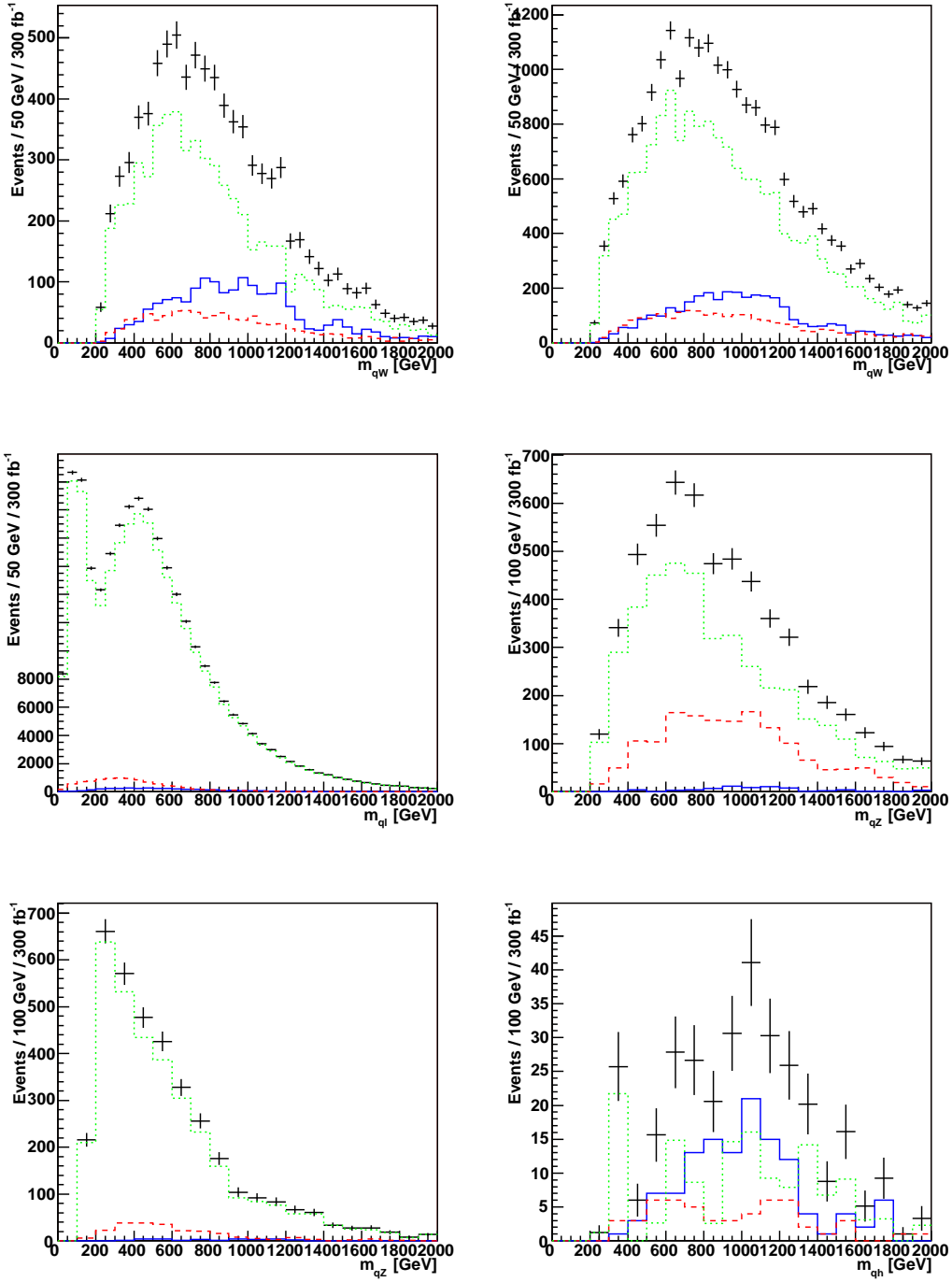
Figure 6: Various invariant mass distributions obtained in a simulation of events for SUSY benchmark scenario γ. See Fig. 4 and text for details.

Figure 7: Various invariant mass distributions obtained in a simulation of events for SUSY benchmark scenario δ. See Fig. 4 and text for details.
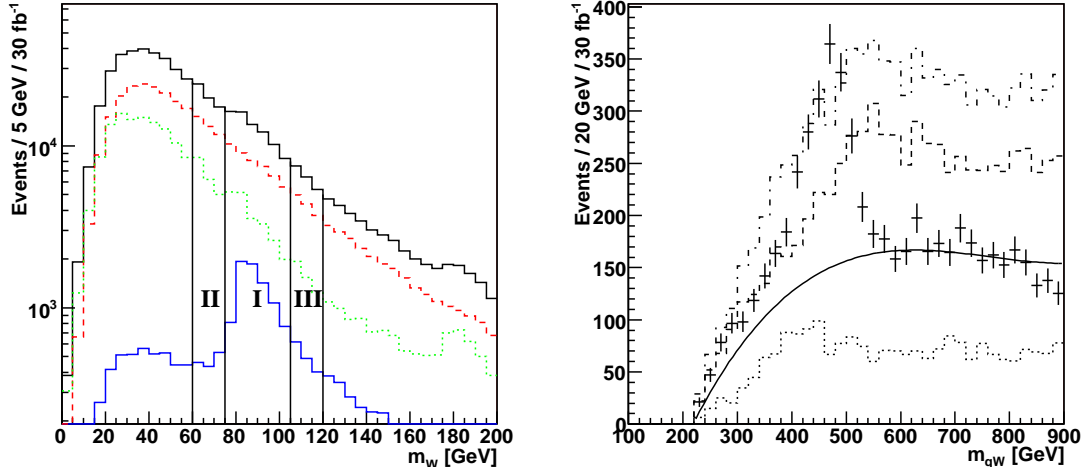
17

Figure 8: Left: Jet mass distribution for W candidates at the α benchmark point following a cut on missing energy: $\not{E}_T > 300$ GeV. The SUSY signal (blue, solid), SUSY background (red, dashed) and SM background (green, dotted) contributions are also shown separately. Right: Invariant mass distribution of qW combinations for the α benchmark point in the signal region (region I, points with error bars), in the sideband regions (region II dashed, region III dotted) and for the sum of sideband events (dashed dotted). Also shown is the fit to the sideband distribution (solid line), rescaled to the signal distribution.

would like to subtract the SM and SUSY backgrounds, without model-dependent assumptions on their shape. We do this by performing a sideband subtraction, where we imitate the background that does not feature a correctly identified boson by collecting a sample of events from the generated "data", that features boson candidates with masses away from the resonance peak of the boson mass in question. Using events in two bands (region II and III) on either side of the signal isolation interval (region I) for the jet mass distribution, each with half the width of the signal band, we recalibrate the boson mass to the nominal peak value as described above, and perform most other cuts as for the signal. The exception is the sub-jet separation scale cut, which is highly correlated with the jet mass cut, and is thus ignored for the sideband sample. We show the jet mass distribution and the signal and sideband regions for W candidates at the α benchmark point in Fig. 8 (left). Only the missing-energy cut given in Section 4.2 has been applied to the events.

The two resulting distributions are added and fitted with a third-degree polynomial, giving the shape of the background. This is shown, again using the α benchmark

18

point as an example, in Fig. 8 (right). The background is rescaled to the full distribution from the signal band, shown with error bars in Figs. 4-7, using bins at higher invariant masses than the observed edges. The rescaled background is then subtracted from the full distributions, the results of which are shown for the qW invariant mass distributions in Fig. 9. While this procedure primarily models background from fake Ws, we find that it does a good job of describing all the background near the upper edges, perhaps with the exception of the δ benchmark point which is dominated by SM events with real Ws. For the other three benchmarks, with much less SM background, the jet rescaling to the W mass for the sideband samples gives a distribution that is similar enough to model well also this background.

We have also considered estimates for the combinatorial background that result from combining correctly identified bosons with the wrong jet, which can be seen as tails in the blue signal distributions in Figs. 4-7. By combining accepted boson and squark decay jet candidates randomly from all events we collect a large mixed sample that should be representative of this part of the background. However, we find that combining these two descriptions of the background is difficult due to the limited statistics, and joint fits to the events in the high invariant-mass region tend to favour heavily the sideband sample. For the δ benchmark point the sideband and mixed samples perform similarly in describing the background in the vicinity of the edge, but the sideband is slightly better at the high invariant masses used to set the scale of the background distribution. As a consequence, the mixed sample is not included in the fits shown in this Section, but investigations into combining different descriptions of the background is certainly worthy of further effort, in particular when data is available from the experiments.

After the sideband subtraction, the upper endpoints of the qW distributions are clearly visible for all four benchmarks in Fig. 9. To estimate their positions, we have performed fits with a linear form for the signal, emulating the distributions of Fig. 3, with a free parameter for the cut-off at the endpoint. These distributions are further smeared by a Gaussian to model the limited jet energy resolution, using a smearing width determined by the fit. The resulting values for the endpoints $m_{qW}^{\max}$ can be found in Table 3. We also show in Fig. 10 the qW invariant mass distributions obtained when we omit the cut on separation scale for the W candidate, and the corresponding fit values are also reported in Table 3.

We see that the endpoint estimates have statistical errors which are in the $\mathcal{O}(1)\%$ region for benchmarks $\alpha - \gamma$ and slightly below $\mathcal{O}(10)\%$ for δ. The statistical errors are in general smaller without the cut on the sub-jet separation scale, particularly in the case of benchmark δ, due to somewhat larger statistics.

In the case of the α benchmark point, the fitted values are both fairly close to the nominal value, but with indications of larger systematic errors when not using
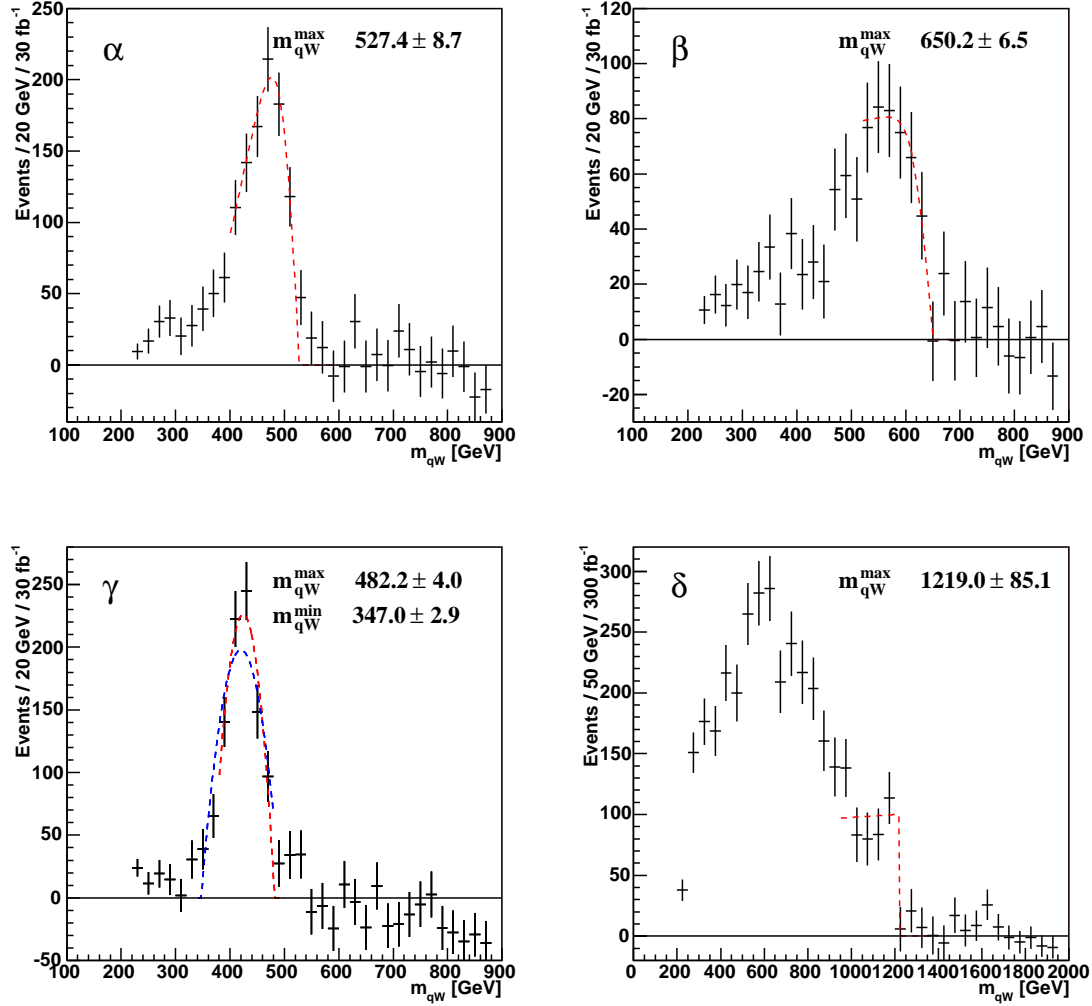
19

Figure 9: Invariant mass distribution of qW combinations at the four benchmark points, α (top left), β (top right), γ (bottom left) and δ (bottom right), after sideband subtraction. Also shown are fits to the upper edges of the distributions, and for γ also the clear lower edge.

Fit / Benchmark	α	β	γ	δ
Scale cut	527.4 ± 8.7	650.2 ± 6.5	482.2 ± 4.0	1219.0 ± 85.1
No scale cut	532.7 ± 3.8	651.5 ± 5.4	481.7 ± 4.1	1203.9 ± 34.5
Nominal	519.9	653.8	468.6	1272.1

Table 3: Fitted endpoint values $m_{qW}^{\max}$ of qW distributions, measured in GeV, compared with the nominal values for the corresponding benchmarks.
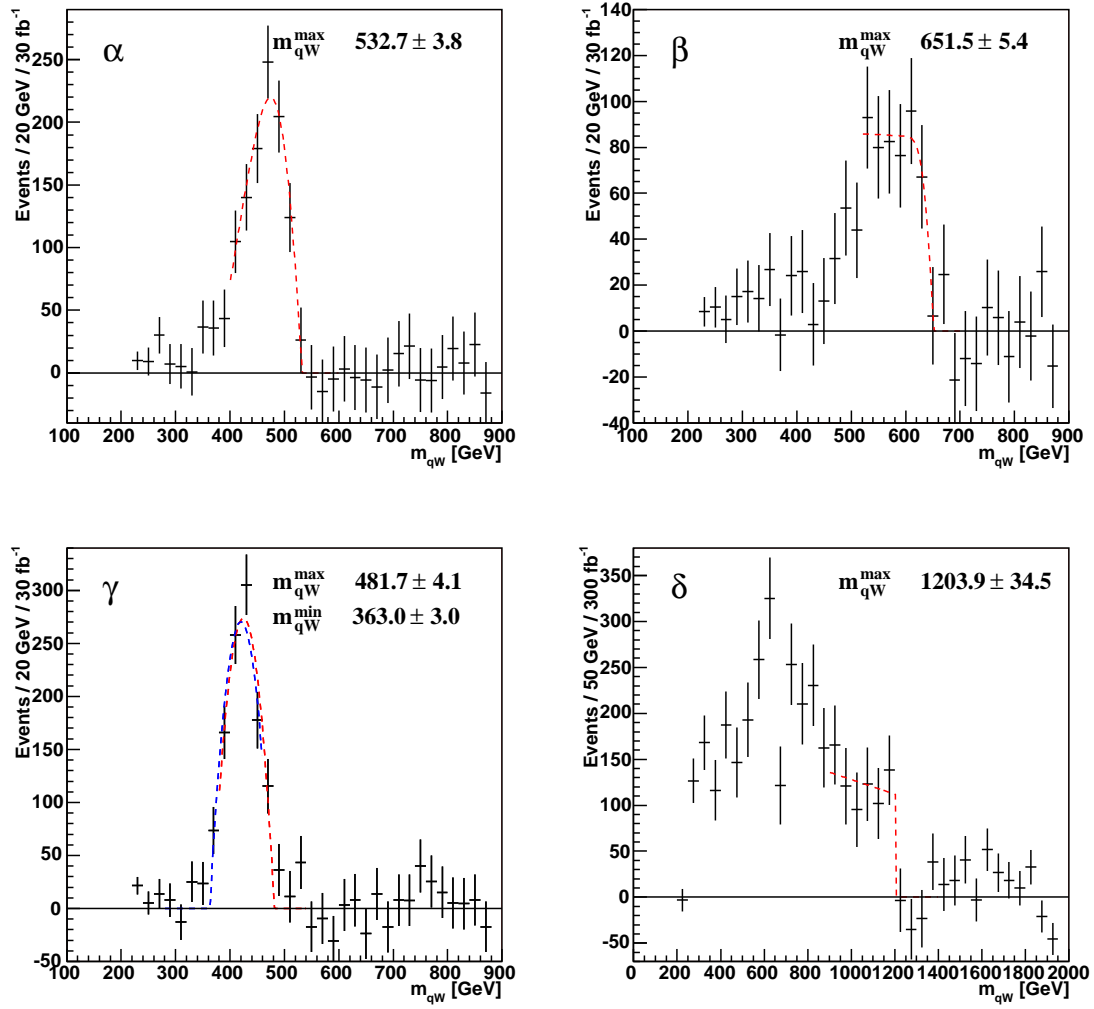
Figure 10: As Fig. 9, but omitting the cut on the sub-jet separation scale.

the scale cut. Both fits overestimate the endpoint, which could be expected as the reconstructed jets from squark decays have not been calibrated for the algorithm's tendency to overestimate the jet. For β both fits are very close to the nominal value, while for γ the fits again overestimate the edge position. From the three benchmarks considered here this systematic error seems to increase for lower values of the endpoint, barring other more important hidden systematics. In the case of the δ benchmark both fits underestimate the endpoint, but here the statistical errors are large. Considered as a whole, the results of Table 3 indicate that the systematical errors on the endpoints in our fitting procedure are comparable to the statistical errors.

For most of the distributions it is impossible to estimate the lower endpoint, since any structure at low invariant masses is washed away by the hard kinematical cuts on jet energies used to isolate the signal. The exception is the relatively high lying lower endpoint of the qW distribution for the γ benchmark, where a similar fitting technique to the one used for the upper endpoint yields a lower endpoint estimate of $m_{qW}^{\min} = 363.0 \pm 3.0$ GeV before and $m_{qW}^{\min} = 347.0 \pm 2.9$ GeV after the sub-jet cut is applied, compared to the nominal value of 369.0 GeV. The difference in endpoint estimate originates from a worse fit of the sideband distribution at high invariant masses when the sub-jet cut is used.

We have in addition estimated both the lower and upper edge of the qZ distribution for the α benchmark point, where we reconstruct the Z from a lepton pair. After a similar sideband subtraction we estimate $m_{qZ}^{\max} = 523.7 \pm 10.6$ GeV and $m_{qZ}^{\min} = 324.5 \pm 9.2$ GeV, to be compared to the nominal values of 505.6 GeV and 358.5 GeV, respectively.

For the qh distributions, fitting is difficult with the low statistics available both at the β and δ benchmarks. From sideband subtracted distributions we make estimates by visual inspection, giving values of $m_{qh}^{\max} = 540 \pm 40$ GeV for β and $m_{qh}^{\max} = 1450 \pm 100$ GeV for δ, compared to the nominal values of 628.3 GeV and 1265.7 GeV, respectively. As has been noted earlier, the feasibility of measuring these edges depends on the b-tagging achievable, and on the use of the sub-jet separation scale cut.

4.5   Mass Spectra

The positions of the edges of the invariant mass distributions may be used to extract information on the spectrum of the SUSY particles involved. Whilst the four equations giving the edges of the qW and qZ/qh distributions may in principle be solved to obtain the four masses involved, extracting accurate values of the absolute masses - as opposed to mass differences - will be difficult in practise because of the degeneracies between the masses of the bosons and of the gauginos,

22

respectively, and thus in the upper edges, as shown in Fig. 3. However, for the four benchmarks considered here this is an academic problem, as neither of the benchmarks have four measurable edges. Given both the lower and upper edge of a single distribution the squark mass can be eliminated from Eq. 4, and one can solve for the mass of the chargino or the next-to-lightest neutralino in terms of the mass of the lightest neutralino. This can in turn be used to arrive at the squark mass. We show in Fig. 11 the squark and $\tilde{\chi}_2^0$ masses determined using the upper and lower qZ edge measured for the α benchmark point, as functions of the undetermined $\tilde{\chi}_1^0$ mass. We also show the 1σ error bands on the masses resulting from the statistical uncertainty of the edge measurements, assuming that the errors on the two edges are independent.

With the squark mass known in terms of the $\tilde{\chi}_1^0$ mass, the upper edge of the qW distribution can also be used to give the $\tilde{\chi}_1^\pm$ mass. Because of the quadratic nature of Eq. 4 two solutions result, none of which can be rejected out of hand [5]. We show both solutions in Fig. 11. For values of the $\tilde{\chi}_1^0$ mass below ~ 50 GeV there are no solutions.

For the γ benchmark point the same procedure can be followed for the two endpoints of the qW distribution, and we show the resulting squark and chargino masses as functions of the lightest neutralino mass in Fig. 12. For the remaining two benchmarks, extracting masses is more difficult since only one edge is well measured. However, the LHC experiments have the potential for measuring other SUSY mass-dependent quantities, such as the effective mass [1, 23], whose determination would give complementary relations between the involved masses.

Given an accurate measurement of the $\tilde{\chi}_1^0$ mass, for example at a future linear collider, the heavier neutralino, chargino and squark masses could then be found with statistical errors in the range of $1-5\%$, using LHC data, even if the particles themselves are too heavy to be produced at the linear collider.

5   Results and Conclusions

We have shown in this paper, we believe for the first time, that it is possible to extract a SUSY signal solely from the hadronic decays of $W^\pm$ bosons produced in cascade decays involving charginos, and that the measurement of this signal may provide useful information about the sparticle mass spectrum. In each of the benchmarks studied, the upper edge of the qW mass distribution in the decay chain $\tilde{q}_L \to \tilde{\chi}_1^\pm q \to \tilde{\chi}_1^0 W^\pm q$ can be measured, with a statistical error of $\mathcal{O}(1)\%$ for the relatively light sparticle masses of benchmarks $\alpha - \gamma$ and $\mathcal{O}(10)\%$ for the heavier δ,

---

[5]There are also in principle two solutions for the $\tilde{\chi}_2^0$ mass, but one can be rejected as unphysical since it is always less than the $\tilde{\chi}_1^0$ mass.
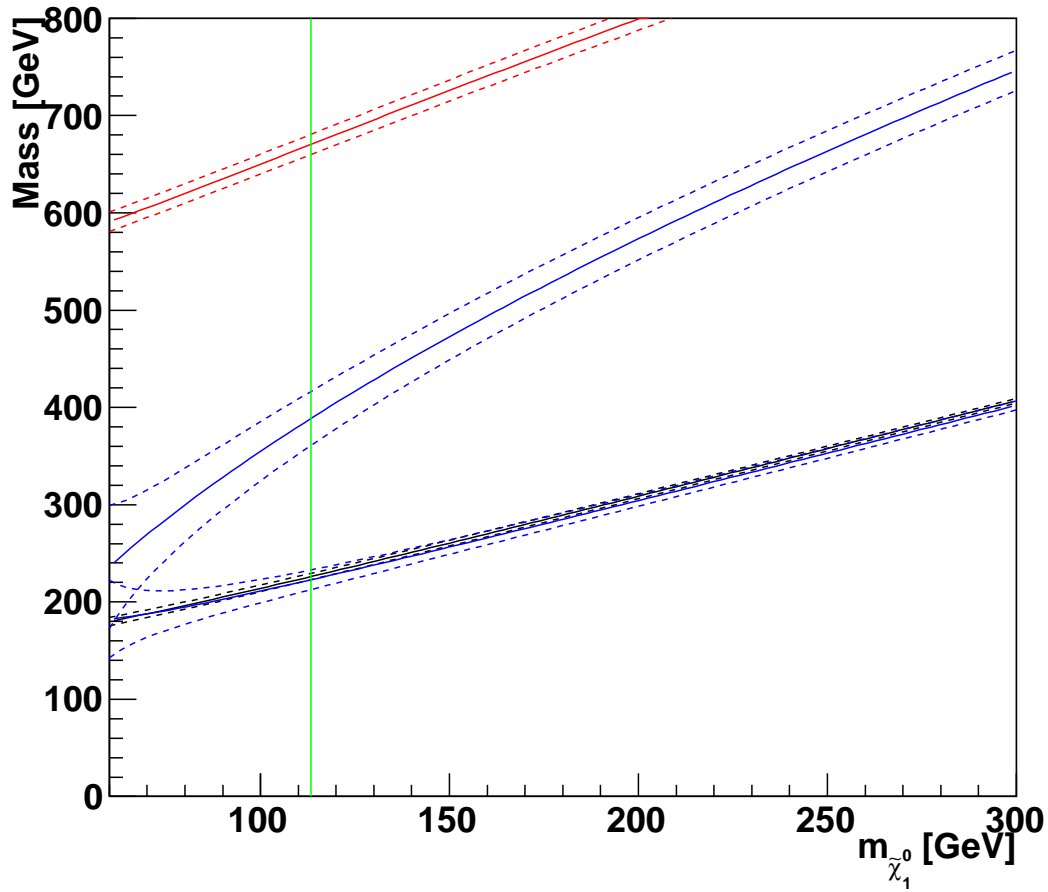
Figure 11: The squark (red), $\tilde{\chi}_1^{\pm}$ (blue) and $\tilde{\chi}_2^0$ (black) masses as a function of the $\tilde{\chi}_1^0$ mass for the α benchmark point. The dashed lines show the 1σ statistical error bands. The vertical green line indicates the nominal $\tilde{\chi}_1^0$ mass.
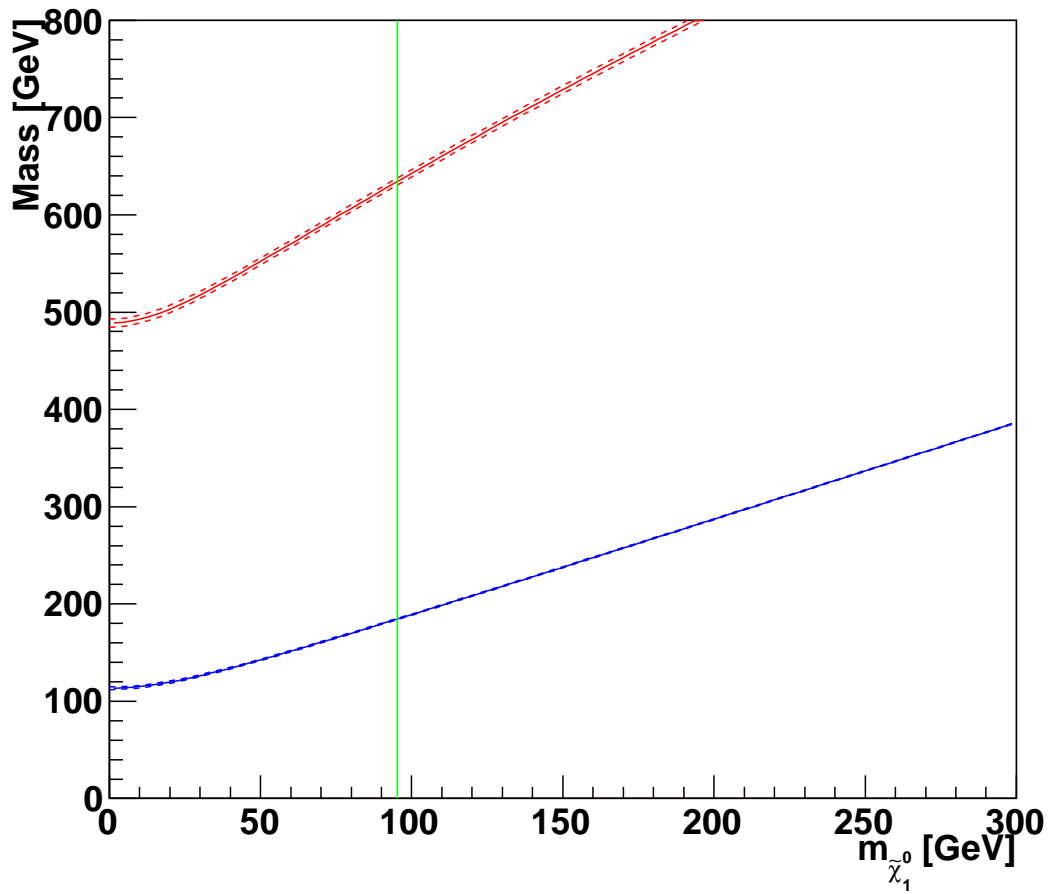
Figure 12: The squark (red) and $\tilde{\chi}_1^{\pm}$ (blue) and masses as a function of the $\tilde{\chi}_1^0$ mass for the γ benchmark point. The dashed lines show the 1σ statistical error bands. The vertical green line indicates the nominal $\tilde{\chi}_1^0$ mass.

with squark and gluino masses above 1.5 TeV. Systematic errors in the background and fitting are estimated to be of the same order as the statistical errors. In the case of benchmark γ, we are also able to extract the position of the lower edge of the qW mass distribution, and in the case of point α we extract both the upper and the lower edges of the qZ mass distribution, using the leptonic decays of Z bosons. There are also clear indications in benchmarks β and δ for the possibility of observing the upper edge of the qh mass distribution using $h \to \bar{b}b$ decays with collimated b-jets, but conclusions on such a signal require further analysis and better understanding of the b-tagging efficiency for these jets in a full detector simulation.

The hadronic signals were extracted using the $K_\perp$ algorithm for jet reconstruction, including the single-jet mass and the proposal of [5] to improve the identification of hadronic decays of heavy bosons via a cut on the sub-jet separation scale. The $K_\perp$ algorithm is shown to be well suited for reconstructing edge features in the considered invariant mass distributions. The sub-jet cut procedure improves quantitatively the signal-to-background ratio, and while the loss of statistics increases the statistical errors, fits to the edges of the qW distribution show improved results with respect to the nominal values when using the sub-jet cut. For the qh distributions with their small signal-to-background ratio, the sub-jet cut is crucial in reducing the background to a manageable level.

A detailed exploration of the capabilities of the LHC experiments to measure and use all the information that could be gained from these benchmark points, and hence a more detailed display of the value added to the global fits by the measurements described here, lies beyond the scope of this study. However, we do note that this technique provides novel information on chargino and neutralino spectroscopy, e.g., the difference between the $\tilde{\chi}_1^0$ and $\tilde{\chi}_1^\pm$ mases, and in at least one case the $\tilde{\chi}_2^0 - \tilde{\chi}_1^\pm$ mass difference. These pieces of information are useful for potentially constraining SUSY models and perhaps foreseeing the locations of interesting thresholds in e^+e^- annihilation.

As pointed out in [5], similar techniques for analysing hadronic final states arising from the decays of heavy particles should be useful in other situations. Examples include the analysis of top physics, the search for R-violating hadronic decays of sparticles, or in the isolation of a generic SUSY signal from QCD SM backgrounds. Indeed, some recent studies have highlighted the potential of single-jet mass cuts in exotic searches [24], and we note that the y-scale cut should also be useful in these cases. We believe this to be an area meriting much further experimental and phenomenological study.

Acknowledgements

References

[1] I. Hinchliffe, F. E. Paige, M. D. Shapiro, J. Soderqvist and W. Yao, Phys. Rev. D **55** (1997) 5520 [arXiv:hep-ph/9610544].

[2] H. Bachacou, I. Hinchliffe and F. E. Paige, Phys. Rev. D **62** (2000) 015009 [arXiv:hep-ph/9907518];
B. C. Allanach, C. G. Lester, M. A. Parker and B. R. Webber, JHEP **0009** (2000) 004 [arXiv:hep-ph/0007009];
C. G. Lester, CERN-THESIS-2004-003;
B. K. Gjelsten, D. J. Miller and P. Osland, JHEP **12** (2004) 003 [arXiv:hep-ph/0410303];
D. J. Miller, P. Osland and A. R. Raklev, JHEP **03** (2006) 034 [arXiv:hep-ph/0510356].

[3] M. M. Nojiri, G. Polesello and D. R. Tovey, arXiv:hep-ph/0312318.

[4] A. De Roeck, J. R. Ellis, F. Gianotti, F. Moortgat, K. A. Olive and L. Pape, [arXiv:hep-ph/0508198].

[5] J. M. Butterworth, B. E. Cox and J. R. Forshaw, Phys. Rev. D **65** (2002) 096014 [arXiv:hep-ph/0201098].

[6] S. Catani, Y. L. Dokshitzer, M. H. Seymour and B. R. Webber, Nucl. Phys. B **406** (1993) 187.

[7] M. Cacciari and G. P. Salam, Phys. Lett. B **641** (2006) 57 [arXiv:hep-ph/0512210].

[8] V. N. Gribov and L. N. Lipatov, Sov. J. Nucl. Phys. **15** (1972) 438 [Yad. Fiz. **15** (1972) 781].
G. Altarelli and G. Parisi, Nucl. Phys. B **126** (1977) 298.
Y. L. Dokshitzer, Sov. Phys. JETP **46** (1977) 641 [Zh. Eksp. Teor. Fiz. **73** (1977) 1216].

[9] T. Sjostrand, S. Mrenna and P. Skands, JHEP **0605**, 026 (2006) [arXiv:hep-ph/0603175]; Note that the events were generated calling PYEVNT,

which uses the same underlying event and parton shower models as the pre-6.3 versions of PYTHIA.

[10] M. L. Mangano et al, JHEP **0307** (2003) 001 [arXiv:hep-ph/0206293]; M. L. Mangano, M. Moretti and R. Pittau, Nucl. Phys. B **632** (2002) 343 [arXiv:hep-ph/0108069]; F. Caravaglios et al, Nucl. Phys. B **539** (1999) 215 [arXiv:hep-ph/9807570].

[11] G. Corcella et al, JHEP 0101 (2001) 010 [arXiv:hep-ph/0011363]; [arXiv:hep-ph/0201201].

[12] J. M. Butterworth, J. R. Forshaw and M. H. Seymour, Z. Phys. C **72** (1996) 637 [arXiv:hep-ph/9601371].

[13] C. Buttar *et al.* in *HERA and the LHC - A workshop on the implications of HERA for LHC physics: Proceedings Part A*, pp.192-217 [arXiv:hep-ph/0601012].

[14] V. M. Abazov *et al.* [D0 Collaboration], Phys. Rev. D **65** (2002) 052008 [arXiv:hep-ex/0108054]; D. Acosta *et al.* [CDF Collaboration], [arXiv:hep-ex/0505013].

[15] S. Chekanov *et al.* [ZEUS Collaboration], Nucl. Phys. B **700** (2004) 3 [arXiv:hep-ex/0405065].

[16] G. Abbiendi *et al.* [OPAL Collaboration], Eur. Phys. J. C **37** (2004) 25 [arXiv:hep-ex/0404026]; Eur. Phys. J. C **31** (2003) 307 [arXiv:hep-ex/0301013]; D. Buskulic *et al.* [ALEPH Collaboration], Phys. Lett. B **384** (1996) 353.

[17] S. Allwood, Manchester University PhD thesis 2005. E. Stefanidis, University College London PhD thesis 2006.

[18] C. L. Bennett *et al.*, Astrophys. J. Suppl. **148** (2003) 1 [arXiv:astro-ph/0302207].

[19] D. N. Spergel *et al.*, Astrophys. J. Suppl. **148** (2003) 175 [arXiv:astro-ph/0302209].

[20] M. Muhlleitner, A. Djouadi and Y. Mambrini, in Comput. Phys. Commun. **168** (2005) 46 [arXiv:hep-ph/0311167].

[21] H. L. Lai *et al.* [CTEQ Collaboration], Eur. Phys. J. C **12** (2000) 375 [arXiv:hep-ph/9903282].

[22] See *HERA and the LHC - A workshop on the implications of HERA for LHC physics: Proceedings Part B*, pp.617-621. [arXiv:hep-ph/0601013]. http://projects.hepforge.org/hztool.

[23] D. R. Tovey, Phys. Lett. B **498** (2001) 1 [arXiv:hep-ph/0006276].

[24] A. L. Fitzpatrick et al, arXiv:hep-ph/0701150;
B. Lillie, L. Randall and L. T. Wang, arXiv:hep-ph/0701166;
W. Skiba and D. Tucker-Smith, arXiv:hep-ph/0701247;
B. Holdom, arXiv:hep-ph/0702037.